Superdirectivity in Linear Holographic MIMO

Andrea Pizzo and Angel Lozano
Universitat Pompeu Fabra, 08018 Barcelona, Spain

***Abstract*—This paper examines mutual coupling in holographic arrays, a novel paradigm where the antenna count and spacings deviate from traditional designs. With only minor deviations from the conventional half-wavelength spacing, strong coupling can accrue as the number of antennas grows large. Properly harnessed, this can lead to a far-field array gain that, on certain directions, increases quadratically (rather than linearly) with that number. Ignored, coupling is bound to manifest itself in unintended manners, some of which are illustrated and discussed.**

I. Introduction

Although array signal processing often regards antennas as independent transducers, the reality is they are inherently coupled by virtue of the exposition to their mutual radiation. However, coupling can be inhibited if each antenna is in a null of the coupling function for every other one. For a uniform linear array (ULA) of omnidirectional antennas, this materializes with an antenna spacing of $d = \frac{\lambda}{2}$ where λ is the wavelength. This is also the spacing that renders the fading at the antennas uncorrelated in isotropic scattering, meaning that the nulls of such fading's spatial correlation coincide with those of the coupling function. The classical design for ULAs is thus to have $d = \frac{\lambda}{2}$, and the far-field directivity or array gain then equals the number of antennas, N.

Enter holographic arrays, an emerging paradigm in which $d < \frac{\lambda}{2}$ and N is very large [1]. By their very nature, such arrays are bound to experience mutual coupling. Indeed, it is well understood how, for $d \to 0$, the coupling surges. What had not been appreciated thus far is that, if d is fixed at some arbitrary value below $\frac{\lambda}{2}$, the mutual coupling also surges as N grows large, in this case owing to the accrual of contributions from an exploding number of antennas. This paper explores this phenomenon and it shows that a slight deviation from $d = \frac{\lambda}{2}$ suffices for strong coupling to build up with N.

Coupling can bring about array gains higher than N, a phenomenon aptly named *superdirectivity* [2]. For $d \to 0$, the gain is known to approach N^2 [3, 4]. For fixed $d < \frac{\lambda}{2}$ and growing N, the gain is herein shown to also scale with N^2, with a scaling factor that depends on $\frac{d}{\lambda}$. While the harnessing of these gains is rife with practical difficulties [5], ignoring coupling is not a sensible alternative because its effects will manifest all the same, only in unintended manners. Recognizing and managing mutual coupling appears altogether imperative in the holographic realm.

II. Directivity of Uniform Linear Arrays

Consider a ULA comprising N single-polarized omnidirectional antennas with $0 < d \leq \frac{\lambda}{2}$. The antennas are driven by a length-N complex current vector $\boldsymbol{j} = (j_0, \ldots, j_{N-1})^{\mathrm{T}}$.

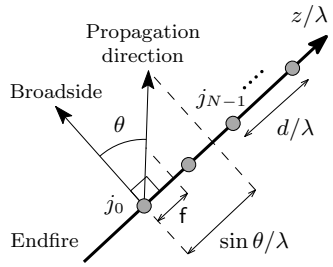

Fig. 1. Geometry of an ULA aligned with the arbitrary z-axis.

Let $\theta \in [-\frac{\pi}{2}, \frac{\pi}{2}]$ be the angle relative to the array's normal direction (see Fig. 1). The discrete spatial frequency $\mathsf{f} = \frac{d}{\lambda} \sin\theta$ is the projection on the array of the propagation vector, of length $\frac{1}{\lambda}$ and direction corresponding to θ, sampled with interval d. It is the frequency along an asymptotically long array of the current induced by a plane wave of wavelength λ arriving on the direction defined by θ or, reciprocally, the frequency along the array of the current that must be excited to radiate on this direction at that wavelength. The windowing effect of an aperture limitation smears each plane wave over a confined angular range or *beam*. Only directions associated with non-overlapping beams are resolvable.

The discrete-space Fourier transform of $\boldsymbol{j}$, is denoted by $J(\mathsf{f})$ and given by

$$J(\mathsf{f}) = \sum_{n=0}^{N-1} j_n \, e^{-\mathrm{j}2\pi\mathsf{f}n} = \boldsymbol{a}^{\mathrm{H}}(\mathsf{f})\, \boldsymbol{j} \tag{1}$$

where

$$\boldsymbol{a}(\mathsf{f}) = \left(1, e^{\mathrm{j}2\pi\mathsf{f}}, \ldots, e^{\mathrm{j}2\pi\mathsf{f}(N-1)}\right)^{\mathrm{T}}. \tag{2}$$

This is spatially bandlimited to $[-\frac{d}{\lambda}, \frac{d}{\lambda}]$, reflecting a lowpass filtering effected by the propagation process; this cuts off the evanescent spectrum, corresponding to spatial frequencies outside that interval that do not contribute real power [6].

Given d, every f maps to an angle θ. This mapping is invertible in $\theta \in [-\frac{\pi}{2}, \frac{\pi}{2}]$, with the sign of f disambiguating mirror directions. Low spatial frequencies correspond to propagation about the broadside direction (normal to the array) whereas high spatial frequencies map to the vicinity of the endfire direction (aligned with the array).

Given some current $\boldsymbol{j}$, the directivity or array gain on a certain direction is defined as the ratio of the power spectral density at the associated f to its average over $[-\frac{d}{\lambda}, \frac{d}{\lambda}]$ (the radiated power), i.e.,

$$G\big(\boldsymbol{j}, \mathsf{f}, \tfrac{d}{\lambda}\big) = \frac{|J(\mathsf{f})|^2}{\frac{\lambda}{2d}\int_{-d/\lambda}^{d/\lambda} |J(\xi)|^2 \, d\xi}. \tag{3}$$

As one would expect, averaging (3) over f returns 1.

III. Uncoupled Antennas

Setting $d = \frac{\lambda}{2}$ results in uncoupled antennas and (3) then specializes to

$$G(\boldsymbol{j},\mathsf{f}) = G(\boldsymbol{j},\mathsf{f},\tfrac{1}{2}) = \frac{|J(\mathsf{f})|^2}{\int_{-1/2}^{1/2}|J(\xi)|^2\,d\xi}. \tag{4}$$

Momentarily considering a uniform current, whose spectrum is the Nth order Dirichlet kernel

$$D_N(\mathsf{f}) = \boldsymbol{a}^{\mathrm{H}}(\mathsf{f})\,\mathbf{1}_N = \frac{\sin(\pi N\mathsf{f})}{\sin(\pi\mathsf{f})}, \tag{5}$$

and using $\int_0^{\frac{\pi}{2}} \frac{\sin^2(Nx)}{\sin^2 x}\,dx = \frac{\pi}{2}N$ for positive integer N, it is found that $G(\mathbf{1}_N,\mathsf{f}) = D_N^2(\mathsf{f})/N$. When $N=1$, a unit gain arises on every direction.

For non-uniform currents, applying Parseval's theorem to the denominator of (4) while replacing the spectrum at the numerator with (1), what emerges is the Rayleigh quotient

$$G(\boldsymbol{j},\mathsf{f}) = \frac{|\boldsymbol{a}^{\mathrm{H}}(\mathsf{f})\boldsymbol{j}|^2}{\|\boldsymbol{j}\|^2} \tag{6}$$

where $\boldsymbol{a}(\mathsf{f})$ is defined in (2).

In the sequel, the superscript * distinguishes the optimum value of any quantity in relation to $\boldsymbol{j}$. In particular, the maximum achievable gain at some f is seen to be

$$G^\star(\mathsf{f}) = \max_{\boldsymbol{j}\neq\mathbf{0}} G(\boldsymbol{j},\mathsf{f}) \tag{7}$$

$$= \lambda_0(\boldsymbol{A}(\mathsf{f})) = N \tag{8}$$

where $\boldsymbol{A}(\mathsf{f}) = \boldsymbol{a}(\mathsf{f})\boldsymbol{a}^{\mathrm{H}}(\mathsf{f})$ such that $\mathrm{tr}(\boldsymbol{A}(\mathsf{f})) = N$, attained—up to a factor due to the scaling invariance of (6)—by

$$\boldsymbol{j}^\star(\mathsf{f}) = \boldsymbol{a}(\mathsf{f}). \tag{9}$$

As expected, in the absence of coupling, the maximum-ratio transmission is optimum.

IV. Impact of Coupling

To isolate the effect of mutual coupling, arising from having $d < \frac{\lambda}{2}$, from the effects of changing the current, $G^\star(\mathsf{f},\frac{d}{\lambda})$ is henceforth normalized by its counterpart for $d = \frac{\lambda}{2}$ into the superdirectivity factor

$$S\big(\mathsf{f},\tfrac{d}{\lambda}\big) = \frac{G^\star(\mathsf{f},\frac{d}{\lambda})}{G^\star(\mathsf{f})} \tag{10}$$

$$= \frac{G^\star(\mathsf{f},\frac{d}{\lambda})}{N}. \tag{11}$$

Setting $d = \frac{\lambda}{2}$ returns $S(\mathsf{f},\frac{1}{2}) = 1\ \forall\mathsf{f}$, a uniform factor in the spatial frequency domain. As seen next, this uniformity breaks down for $d < \frac{\lambda}{2}$ due to the surge in mutual coupling [7].

A. Superdirectivity

Multiplying and dividing (3) by $\int_{-1/2}^{1/2}|J(\xi)|^2\,d\xi > 0$, it follows that

$$G\big(\boldsymbol{j},\mathsf{f},\tfrac{d}{\lambda}\big) = \frac{G(\boldsymbol{j},\mathsf{f})}{C(\boldsymbol{j},\frac{d}{\lambda})} \tag{12}$$

where $G(\cdot)$ is given by (4) and $C(\cdot)$ is defined by

$$C(\boldsymbol{j},\tfrac{d}{\lambda}) = \frac{\frac{\lambda}{2d}\int_{-d/\lambda}^{d/\lambda}|J(\xi)|^2\,d\xi}{\int_{-1/2}^{1/2}|J(\xi)|^2\,d\xi}. \tag{13}$$

Focusing on $C(\boldsymbol{j},\frac{d}{\lambda})$, applying Parseval's theorem to the numerator while integrating at the denominator, namely

$$\int_{-d/\lambda}^{d/\lambda} e^{-\mathrm{j}2\pi f n}\,df = \frac{\sin\big(2\pi\frac{d}{\lambda}n\big)}{\pi n} = \omega_n(\tfrac{d}{\lambda}), \tag{14}$$

what emerges is the Rayleigh quotient

$$C\big(\boldsymbol{j},\tfrac{d}{\lambda}\big) = \frac{\boldsymbol{j}^{\mathrm{H}}\boldsymbol{C}(\frac{d}{\lambda})\boldsymbol{j}}{\|\boldsymbol{j}\|^2} \tag{15}$$

where $\boldsymbol{C}$ is a symmetric Toeplitz matrix, positive-definite,

$$\boldsymbol{C}(\tfrac{d}{\lambda}) = \tfrac{\lambda}{2d}\,\boldsymbol{\Omega}(\tfrac{d}{\lambda}), \tag{16}$$

with $\boldsymbol{\Omega} = \{\omega_{n-m};\, n,m = 0,\ldots,N-1\}$ the prolate matrix [8].

Combining (15), (12), and (6), the gain with coupled antennas emerges as the generalized Rayleigh quotient

$$G\big(\boldsymbol{j},\mathsf{f},\tfrac{d}{\lambda}\big) = \frac{\boldsymbol{j}^{\mathrm{H}}\boldsymbol{A}(\mathsf{f})\boldsymbol{j}}{\boldsymbol{j}^{\mathrm{H}}\boldsymbol{C}(\frac{d}{\lambda})\boldsymbol{j}}. \tag{17}$$

Letting λ_k and $\boldsymbol{v}_k$ be the ordered eigenvalues and associated eigenvectors of the generalized eigenvalue problem

$$\boldsymbol{A}(\mathsf{f})\,\boldsymbol{v}_k = \lambda_k\,\boldsymbol{C}\big(\tfrac{d}{\lambda}\big)\,\boldsymbol{v}_k \qquad k = 0,\ldots,N-1, \tag{18}$$

the maximum of (17) is given by

$$G^\star\big(\mathsf{f},\tfrac{d}{\lambda}\big) = \lambda_0\big(\boldsymbol{C}^{-1}\big(\tfrac{d}{\lambda}\big)\boldsymbol{A}(\mathsf{f})\big), \tag{19}$$

attained by $\boldsymbol{j}^\star = \boldsymbol{v}_0$ (which is a function of f and $\frac{d}{\lambda}$). Since $\boldsymbol{A}(\mathsf{f})$ is of rank-1, λ_0 is actually the only positive eigenvalue and thus

$$G^\star\big(\mathsf{f},\tfrac{d}{\lambda}\big) = \boldsymbol{a}(\mathsf{f})^{\mathrm{H}}\,\boldsymbol{C}^{-1}(\tfrac{d}{\lambda})\,\boldsymbol{a}(\mathsf{f}), \tag{20}$$

attainable, up to a factor, by

$$\boldsymbol{j}^\star\big(\mathsf{f},\tfrac{d}{\lambda}\big) = \boldsymbol{C}^{-1}\big(\tfrac{d}{\lambda}\big)\,\boldsymbol{a}(\mathsf{f}). \tag{21}$$

It follows that the superdirectivity factor in (10) satisfies

$$S\big(\mathsf{f},\tfrac{d}{\lambda}\big) = \frac{1}{N}\,\boldsymbol{a}(\mathsf{f})^{\mathrm{H}}\boldsymbol{C}^{-1}(\tfrac{d}{\lambda})\,\boldsymbol{a}(\mathsf{f}), \tag{22}$$

which, averaged over f, gives

$$\overline{S}\big(\tfrac{d}{\lambda}\big) = \frac{\lambda}{2d}\int_{-d/\lambda}^{d/\lambda} S\big(\mathsf{f},\tfrac{d}{\lambda}\big)\,d\mathsf{f} \tag{23}$$

$$= \frac{1}{N}\,\mathrm{tr}\left(\boldsymbol{C}^{-1}\big(\tfrac{d}{\lambda}\big)\,\frac{\lambda}{2d}\int_{-d/\lambda}^{d/\lambda}\boldsymbol{A}(\mathsf{f})\,d\mathsf{f}\right) \tag{24}$$

$$= \frac{1}{N}\,\mathrm{tr}\big(\boldsymbol{C}^{-1}\big(\tfrac{d}{\lambda}\big)\,\boldsymbol{C}\big(\tfrac{d}{\lambda}\big)\big) = 1 \tag{25}$$

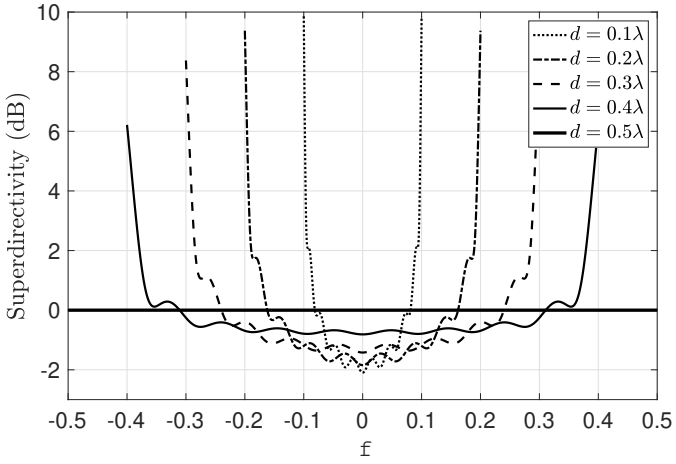

Fig. 2. Superdirectivity $S(\mathsf{f}, \frac{d}{\lambda})$ in dB as a function of the spatial frequency for various antenna spacings. ULA with $N = 10$ omnidirectional antennas.

where $\boldsymbol{C}(\frac{d}{\lambda}) = \frac{\lambda}{2d}\int_{-d/\lambda}^{d/\lambda} \boldsymbol{A}(\mathsf{f})\, d\mathsf{f}$ was used, as derivable from (2), and (14) was recalled. Thus, coupling merely redistributes the maximum gain as a function of f. This is exemplified in Fig. 2 where $S(\mathsf{f}, \frac{d}{\lambda})$ is plotted as a function of f for $N = 10$ antennas and various $\frac{d}{\lambda}$. As d falls below $\frac{\lambda}{2}$, coupling arises, redistributing power towards the endfire directions, with the superdirectivity approaching a value of N as $\frac{d}{\lambda} \to 0$ [3, 4].

B. Practical Challenges

Denoting by $\lambda_k(\boldsymbol{\Omega})$ and $\boldsymbol{u}_k(\frac{d}{\lambda})$ the ordered eigenvalues and associated eigenvectors of the prolate matrix $\boldsymbol{\Omega}$, $\boldsymbol{u}_k(\frac{d}{\lambda})$ equals the truncation to $n = 0, \ldots, N-1$ of the discrete prolate spheroidal sequence of order k, $u_n^{(k)}(\frac{d}{\lambda})$ [8]. Furthermore, the discrete prolate spheroidal wave function $U_k(\mathsf{f}, W)$ is found as the Fourier transform of $\boldsymbol{u}_k(\frac{d}{\lambda})$, namely [8, Eq. 26]

$$U_k(\mathsf{f}, \tfrac{d}{\lambda}) = \epsilon_k\, e^{-\mathrm{j}\pi(N-1)\mathsf{f}} \boldsymbol{a}^{\mathrm{H}}(\mathsf{f})\, \boldsymbol{u}_k\big(\tfrac{d}{\lambda}\big) \tag{26}$$

for $k = 0, \ldots, N-1$, with ϵ_k being 1 or j according to k being even or odd, ensuring that (26) is real-valued. The spectra $\{U_k(\mathsf{f}, \frac{d}{\lambda})\}$ are symmetric, periodic, orthogonal in $[-\frac{d}{\lambda}, \frac{d}{\lambda}]$ with average energy $\lambda_k(\boldsymbol{\Omega})$, and orthonormal in $[-\frac{1}{2}, \frac{1}{2}]$.

While the eigenvectors of $\boldsymbol{\Omega}$ are unaltered by the scaling in (16), the eigenvalues are related to the ones of $\boldsymbol{C}$ by $\lambda_k(\boldsymbol{\Omega}) = \frac{2d}{\lambda}\lambda_k(\boldsymbol{C})$. Then, replacing $\boldsymbol{C}$ with its eigenvalue decomposition, (22) morphs into

$$S\big(\mathsf{f}, \tfrac{d}{\lambda}\big) = \frac{1}{N}\sum_{k=0}^{N-1} \frac{1}{\lambda_k(\boldsymbol{C})} \left|\boldsymbol{a}^{\mathrm{H}}(\mathsf{f})\, \boldsymbol{u}_k\big(\tfrac{d}{\lambda}\big)\right|^2 \tag{27}$$

$$= \frac{1}{N}\sum_{k=0}^{N-1} \frac{1}{\lambda_k(\boldsymbol{C})} U_k^2\big(\mathsf{f}, \tfrac{d}{\lambda}\big) \tag{28}$$

where (26) was used. The superdirectivity factor has contributions from every prolate spheroidal wave function as per their orthogonality. From (21), in the same vein of (28),

$$\boldsymbol{j}^\star\big(\mathsf{f}, \tfrac{d}{\lambda}\big) = e^{\mathrm{j}\pi(N-1)\mathsf{f}} \sum_{k=0}^{N-1} \frac{U_k\big(\mathsf{f}, \frac{d}{\lambda}\big)}{\epsilon_k \lambda_k(\boldsymbol{C})}\, \boldsymbol{u}_k\big(\tfrac{d}{\lambda}\big)\,, \tag{29}$$

where, recall, ϵ_k equals 1 or j. Then, from (1),

$$J^\star\big(\xi, \mathsf{f}, \tfrac{d}{\lambda}\big) = \sum_{k=0}^{N-1} \frac{(-1)^k}{\lambda_k(\boldsymbol{C})}\, U_k\big(\mathsf{f}, \tfrac{d}{\lambda}\big)\, U_k\big(\xi, \tfrac{d}{\lambda}\big) \tag{30}$$

as a function of the spatial frequency ξ given an f for which the current is optimized.

Upper and lower bounds on (28) are obtained by equating $\boldsymbol{a}(\mathsf{f})/\sqrt{N}$ to $\boldsymbol{u}_{N-1}(\frac{d}{\lambda})$ and $\boldsymbol{u}_0(\frac{d}{\lambda})$, respectively, whereby

$$\frac{1}{\lambda_0(\boldsymbol{C})} \le S\big(\mathsf{f}, \tfrac{d}{\lambda}\big) \le \frac{1}{\lambda_{N-1}(\boldsymbol{C})} \tag{31}$$

for any f. Thus, large variations in the superdirectivity are possible when $\boldsymbol{C}$ is ill-conditioned, which in turn occurs when the coupling is strong. Precisely, high superdirectivities are achieved on those spatial frequencies for which $\boldsymbol{a}(\mathsf{f})$ contains a portion of the nullspace of $\boldsymbol{C}$. The maximum variation is quantified by the conditioning number $\lambda_0(\boldsymbol{C})/\lambda_{N-1}(\boldsymbol{C})$. However, achieving extreme superdirectivities requires driving an array with potentially enormous currents as per (21). The poor conditioning also provides an unstable solution that is sensitive to small changes in its entries, say in the antenna excitations and positions [5]. Numerically, this difficulty in inverting $\boldsymbol{C}$ in (20) maps to the ill-conditioning of (18) due to $\boldsymbol{A}$ being almost completely null and its null-space intersecting with the one of $\boldsymbol{C}$ [9].

C. Realizable Superdirectivity

Robustness is gained as the lossless antennas considered thus far are replaced by their lossy brethren, making superdirectivity accessible in practice [7]. Such losses amount to an additional term that incorporates the power dissipated as heat, subsumed in the augmented matrix

$$\boldsymbol{C}\big(\tfrac{d}{\lambda}, \eta\big) = \Big(\tfrac{1}{\eta} - 1\Big)\, \boldsymbol{I}_N + \boldsymbol{C}\big(\tfrac{d}{\lambda}\big) \tag{32}$$

where $0 < \eta \le 1$ is the antenna radiation efficiency and $\boldsymbol{C}(\frac{d}{\lambda})$ corresponds to lossless antennas. Through η, the losses act as a physical regularization, improving the conditioning of $\boldsymbol{C}(\frac{d}{\lambda})$.

While the eigenvectors are not altered by this regularization, the eigenvalues of (32) do change into

$$\lambda_k(\boldsymbol{C}, \eta) = \Big(\tfrac{1}{\eta} - 1\Big) + \lambda_k(\boldsymbol{C}) \tag{33}$$

where $\lambda_k(\boldsymbol{C})$ is associated with lossless antennas. Expectedly, a trade-off arises between maximum superdirectivity, for $\eta = 1$, and physical realizability, corresponding to $\eta < 1$ and a surging dissipated power. Antenna losses raise the eigenvalue threshold that activates superdirectivity, improving reliability but taking a toll on the gains. The dependence of the superdirectivity on η is made explicit by $S(\mathsf{f}, \frac{d}{\lambda}, \eta)$, such that $S(\mathsf{f}, \frac{d}{\lambda}, 1) = S(\mathsf{f}, \frac{d}{\lambda})$ corresponds to lossless antennas.

V. Wide Apertures

As seen, superdirectivity arises when $\boldsymbol{C}$ is of reduced rank, reflecting a build-up in coupling. For a given number of antennas, N, this occurs with shrinking $\frac{d}{\lambda}$ [7]. However, coupling

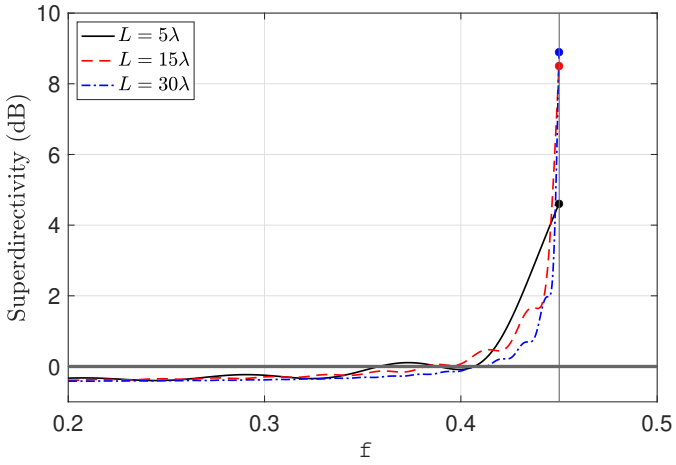

Fig. 3. Superdirectivity $S(\mathsf{f}, \frac{d}{\lambda})$ in dB as a function of the spatial frequency for various apertures. ULA with omnidirectional antennas spaced by $d = 0.45\lambda$ and efficiency $\eta = 0.9999$.

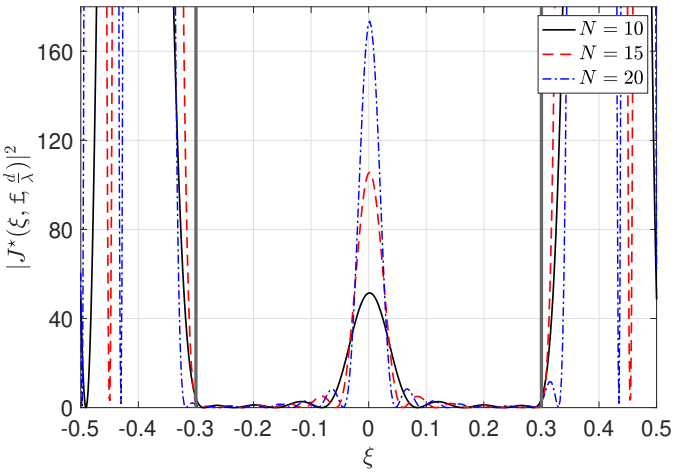

Fig. 4. Approximation of a delta function at $\mathsf{f} = 0$ over $\xi \in [-0.3, 0.3]$ for various N up to an accuracy of $\eta = 0.9999$.

also strengthens as N grows with fixed $\frac{d}{\lambda}$, corresponding to a widening aperture at the scale of λ.

As N increases, the eigenvalues of $\boldsymbol{C}$ polarize into two levels, with the transition occurring approximately at [8]

$$r(\boldsymbol{C}) = \left\lfloor 2\tfrac{d}{\lambda} N \right\rfloor \approx \left\lfloor 2\tfrac{L}{\lambda} \right\rfloor, \tag{34}$$

irrespectively of the antenna efficiency. Alternatively, (34) is obtainable by leveraging the asymptotic equivalence between Toeplitz matrices and circulant matrices (see App. A) or by pursuing a signal-space approach, whereby this transition point can be identified with the number of spatial degrees of freedom [10]. Indeed, $r(\boldsymbol{C})$ specifies the number of antennas that are essentially uncoupled, asymptotically in N. Put differently, the array with N partially coupled antennas is equivalent, in the sense of the associated $\boldsymbol{C}$ matrices having the same eigenvalues, to another hypothetical array with $r(\boldsymbol{C})$ uncoupled antennas and $N - r(\boldsymbol{C}) = N(1 - 2\frac{d}{\lambda})$ fully coupled ones. Since fully coupled antennas generate a quadratic endfire gain [3, 4], it follows that, for fixed $\frac{d}{\lambda}$ and growing N, the gain is $\alpha(\frac{d}{\lambda})N^2$ with $\alpha(\frac{d}{\lambda}) \to 1$ as $\frac{d}{\lambda} \to 0$.

This phenomenon is illustrated in Fig. 3 where $S(\mathsf{f}, \frac{d}{\lambda}, \eta)$ is plotted as a function of f for $L = \{5, 15, 30\}\lambda$ and $\eta = 0.9999$. Antennas are spaced by $d = 0.45\lambda$, evidencing that coupling can be strong with d deviating only slightly from $\frac{\lambda}{2}$.

A. Superdirectivity and Superoscillations

From (3), an unbounded array gain appears attainable by a singularly-integrable power spectral density, the likes of a delta function $\delta(\xi - \mathsf{f})$ for any $|\mathsf{f}| \leq \frac{1}{2}$. Yet approximating such a spectrum with arbitrary accuracy requires asymptotically many samples as per the sampling theorem. With a finite number of samples, N, the power spectral density can only approximate a delta function. As shown in App. B, for $\eta = 1$, the minimum-power approximation (yielding the highest gain) is given by

$$|J^\star\big(\xi, \mathsf{f}, \tfrac{d}{\lambda}\big)|^2 = |D_N(\xi - \mathsf{f})|^2 \, \Pi_N(\xi, \mathsf{f}, \tfrac{d}{\lambda}) \tag{35}$$

as a function of ξ for any given f. Here,

$$\Pi_N(\xi, \mathsf{f}, \tfrac{d}{\lambda}) = \big(2\tfrac{d}{\lambda}\big)^2 \mathbb{1}_{\left\{|\xi| \leq \frac{d}{\lambda}\right\}} \tag{36}$$

reflects the band-limitation, with $\mathbb{1}_{\mathcal{X}}$ the indicator function of a set $\mathcal{X}$. Letting $N \to \infty$, the power density tends to $\delta(\xi - \mathsf{f})$ by virtue of the Dirichlet kernel convergence. Reintroducing antenna losses increases the power needed for a given approximation, or decreases the accuracy for the same power. For instance, the power density $|J^\star(\xi, \mathsf{f}, \frac{d}{\lambda})|^2$ in (30) is plotted in Fig. 4 for $\mathsf{f} = 0$, $d = 0.3\lambda$, $N = \{10, 15, 20\}$, and $\eta = 0.9999$. The oscillatory behavior of the Dirichlet kernel within the spatial bandwidth is readily apparent. Also, notice how fashioning current spectra that boost superdirectivity, subject to a certain radiated power, entails wild behaviors on the interval of evanescent waves, $\frac{d}{\lambda} < |\xi| < \frac{1}{2}$, which do not contribute to that power. These enormous currents produce high field intensities within the reactive near field of the array, incurring in power dissipation through antenna losses. This surge in power can be understood through a phenomenon called superoscillation [11], which allows for a length-N current vector to accelerate the rate of change of its spectrum arbitrarily—to fit the extreme oscillations elicited by the Dirichlet kernel—provided it does so only locally, within the spatial bandwidth, and without violating the sampling theorem on average.

VI. Unintended Superdirectivity

Coupling may arise even for $d = \frac{\lambda}{2}$. This is the case in planar arrays, where coupling builds up along the northeast, southeast, southwest, and northwest directions, on which antennas are spaced at multiples of $\frac{\lambda}{\sqrt{2}}$. It is also the case in wideband transmissions, when the signal occupies $f \in [f_{\min}, f_{\max}]$ (in Hz) and the maximum frequency deviation $\Delta = \frac{(f_{\max} - f_{\min})}{f_{\max}}$ is nonnegligible. Then, $\frac{d}{\lambda}$ varies over the transmission bandwidth. The implication of this frequency dependence is showcased in Fig. 5, which depicts the ratio between the endfire and broadside superdirectivities as a function

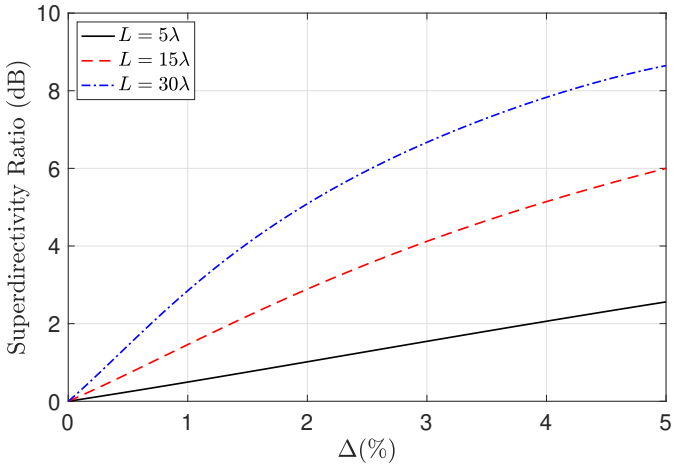

Fig. 5. Ratio between the endfire and broadside superdirectivities (in dB) as a function of the frequency shift (in percentage) for various apertures. ULA with antennas spaced by $d = \frac{\lambda}{2}$ at $f_{\max}$, and efficiency $\eta = 0.9999$.

of Δ for various apertures when $d = \frac{\lambda}{2}$ at $f_{\max}$. For 5G NR operating at $\frac{f_{\max}+f_{\min}}{2} = 28$ GHz with $f_{\max} - f_{\min} = 400$ MHz, for instance, $\Delta = 1.4\%$; for $L = 30\lambda$ there is then a 4-dB shift in gain from broadside to endfire over the signal bandwidth. This introduces frequency-domain distortion that adds to whatever frequency selectivity the channel exhibits.

Acknowledgment

Work supported by MICIU under the Maria de Maeztu Units of Excellence Programme (CEX2021-001195-M), by ICREA, and by AGAUR (Catalan Government).

Appendix A

For large N, the unordered eigenvalues of $\boldsymbol{C}$ in (16) approach the discrete Fourier transform coefficients of $\{c_n\} = \{\frac{\lambda}{2d}\omega_n\}$ with ω_n in (14) [12]. Such eigenvalues are thus obtainable by sampling the associated spectrum $\frac{\lambda}{2d}\mathbb{1}_{\{|\mathsf{f}|\le d/\lambda\}}$ in $|\mathsf{f}| \le \frac{1}{2}$ with spacing $\mathsf{f} = \frac{k}{N}$ for positive integer k, whereby

$$\lambda_k(\boldsymbol{C}) \approx \begin{cases} \frac{\lambda}{2d} & k = 0, 1, \ldots, 2\frac{d}{\lambda}N - 1 \\ 0 & k = 2\frac{d}{\lambda}N, \ldots, N-1 \end{cases} \tag{37}$$

where the approximation sharpens with N. Then, substituting (34) while accounting for antenna losses through (33) yields

$$\lambda_k(\boldsymbol{C}, \eta) \approx \begin{cases} (\frac{1}{\eta} - 1) + \frac{N}{r(\boldsymbol{C})} & k = 0, 1, \ldots, r(\boldsymbol{C}) - 1 \\ (\frac{1}{\eta} - 1) & k = r(\boldsymbol{C}), \ldots, N-1. \end{cases} \tag{38}$$

Appendix B

The minimum-power signal $f(z)$, spatially bandlimited to $\frac{2}{\lambda}$ and passing through $f(kd) = f_k$, $k = 0, \ldots, N-1$, is [13]

$$f(z) = \sum_{n=0}^{N-1} x_n \operatorname{sinc}\big(\tfrac{2}{\lambda}(z - nd)\big) \tag{39}$$

with $\boldsymbol{x} = (x_0, \ldots, x_{N-1})^{\mathrm{T}}$ satisfying

$$\boldsymbol{C}(\tfrac{d}{\lambda})\,\boldsymbol{x} = \boldsymbol{f} \tag{40}$$

where $\boldsymbol{C}$ is defined in (16) and $\boldsymbol{f} = (f_0, \ldots, f_{N-1})^{\mathrm{T}}$. Setting $d = \frac{\lambda}{2}$ while letting $N \to \infty$, (39) specializes to the sampling theorem whereby the expansion coefficients expectedly become the Nyquist samples $x_k = f(k\frac{\lambda}{2})$ $\forall k$.

Comparing (40) against (21) unveils $\boldsymbol{f} = \boldsymbol{a}(\mathsf{f})$ in (2) and that $\boldsymbol{x} = \boldsymbol{j}^\star(\mathsf{f}, \frac{d}{\lambda})$ at every f. Then, sampling (39) at $z = kd$,

$$e^{\mathrm{j}2\pi\mathsf{f}k} = \sum_{n=0}^{N-1} j_n^\star\big(\mathsf{f}, \tfrac{d}{\lambda}\big)\, \operatorname{sinc}\big(2\tfrac{d}{\lambda}(k-n)\big) \tag{41}$$

for $k = 0, \ldots, N-1$. Further taking the discrete-space Fourier transform of both sides of (41) gives, by convolution theorem,

$$D_N(\xi - \mathsf{f}) = \frac{\lambda}{2d}\mathbb{1}_{\{|\xi|\le\frac{d}{\lambda}\}}\, e^{-\mathrm{j}\pi(\xi-\mathsf{f})(N-1)} \boldsymbol{a}^{\mathrm{H}}(\xi)\boldsymbol{j}^\star\big(\mathsf{f}, \tfrac{d}{\lambda}\big) \tag{42}$$

$$= \frac{\lambda}{2d}\mathbb{1}_{\{|\xi|\le\frac{d}{\lambda}\}}\, e^{-\mathrm{j}\pi(\xi-\mathsf{f})(N-1)}\, J^\star\big(\xi, \mathsf{f}, \tfrac{d}{\lambda}\big) \tag{43}$$

as a function ξ for any given f, where (1) was used. Rearranging (43) and squaring the resulting expressions yields (35).

References

[1] E. Björnson *et al.*, "Massive MIMO is a reality—what is next?: Five promising research directions for antenna arrays," *Dig. Sig. Process.*, vol. 94, pp. 3–20, 2019.

[2] R. Harrington, "On the gain and beamwidth of directional antennas," *IRE Trans. Ant. Prop.*, vol. 6, no. 3, pp. 219–225, 1958.

[3] A. Uzkov, "An approach to the problem of optimum directive antenna design," *Comptes Rendus de l'Academie des Sci. de l'URSS*, vol. 53, no. 1, pp. 35–38, 1946.

[4] E. E. Altshuler *et al.*, "A monopole superdirective array," *IEEE Trans. Ant. Prop.*, vol. 53, no. 8, pp. 2653–2661, 2005.

[5] E. N. Gilbert and S. P. Morgan, "Optimum design of directive antenna arrays subject to random variations," *The Bell Syst. Tech. J.*, vol. 34, no. 3, pp. 637–663, 1955.

[6] T. B. Hansen and A. D. Yaghjian, *Plane-Wave Theory of Time-Domain Fields*. Wiley-IEEE Press, 1999.

[7] M. T. Ivrlač and J. A. Nossek, "Toward a circuit theory of communication," *IEEE Trans. Circuits and Systems*, vol. 57, no. 7, pp. 1663–1683, 2010.

[8] D. Slepian, "Prolate spheroidal wave functions, Fourier analysis, and uncertainty — V: The discrete case," *The Bell Syst. Techn. J.*, vol. 57, no. 5, pp. 1371–1430, 1978.

[9] G. H. Golub, "Some modified matrix eigenvalue problems," *SIAM Review*, vol. 15, no. 2, pp. 318–334, 1973.

[10] A. S. Y. Poon *et al.*, "Degrees of freedom in multiple-antenna channels: a signal space approach," *IEEE Trans. Inf. Theory*, vol. 51, no. 2, pp. 523–536, 2005.

[11] P. J. S. G. Ferreira and A. Kempf, "Superoscillations: Faster than the Nyquist rate," *IEEE Trans. Sig. Process.*, vol. 54, no. 10, pp. 3732–3740, 2006.

[12] R. M. Gray, *Toeplitz and circulant matrices: A review*. Found. Trends Comm. Inf. Theory, 2006, vol. 2, no. 3.

[13] L. Levi, "Fitting a bandlimited signal to given points," *IEEE Trans. Inf. Theory*, vol. 11, no. 3, pp. 372–376.